JOM, Vol. 73, No. 1, 2021
https://doi.org/10.1007/s11837-020-04421-z

Thermodynamics Models for V-pit Nucleation and Growth in III-Nitride on Silicon

KHALED H. KHAFAGY,[1,2] TAREK M. HATEM ,[1,3,4] and SALAH M. BEDAIR[2]

1.—Centre for Simulation Innovation and Advanced Manufacturing, The British University in Egypt, El-Sherouk City, Cairo 11837, Egypt. 2.—Department of Electrical and Computer Engineering, North Carolina State University, Raleigh, NC 27695, USA. 3.—Faculty of Energy and Environmental Engineering, The British University in Egypt, El-Sherouk City, Cairo 11837, Egypt. 4.—e-mail: tarek.hatem@bue.edu.eg

Silicon and sapphire are common substrates for AlN, InGaN, and GaN thin films in several applications such as photovoltaic and light-embedded diodes. Threading dislocations are generated at interfaces between III-nitride (III-N) layers and these substrates because of large lattice and thermal expansion coefficient (TEC) mismatches. These dislocations penetrate the top surface of III-N layers to relax the system by forming V-pit defects. This work presents a thermodynamics-based model to study V-pit formation and growth in InGaN/GaN epilayers on either silicon or sapphire substrates. The model calculates the evolution of V-pit defects in thin films through the energy balance between the strain energy in the III-N layer, dislocation deterioration energy to form new V-pits, and V-pit facet energies that result because of facet formations. The impact of different lattice and TEC mismatches as well as a novel approach, the embedded void approach, on V-pit nucleation and growth is also investigated.

INTRODUCTION

In the last decades, the III-nitride (III-N) family shows significant improvements in several electronic applications, such as solar cells and light-embedded diodes (LED). However, still the common challenge is to grow III-N materials on lattice-matched substrates, where the cost and difficulties of growing bulk III-N single-grain layers are always the main barriers. Silicon (Si) and sapphire materials are common substrates for several III-N structure cells, where silicon is used as a substrate for AlN, GaN, and InGaN in LED and photovoltaic applications, and sapphire is commonly used as a substrate for GaN in LED applications.[1,2] Since different layers with incoherent interfaces have different lattice structures and constants have been introduced, these large mismatches in both the lattice and thermal expansion coefficient between III-N layers and the substrates generate defects with high densities such as threading dislocations. Such defects are commonly generated at the interface between different layers, where the defects penetrate the top surface of the III-N thin film under harsh growth conditions, affecting the surface morphology and roughness. Common defects such as V-pits are commonly generated on the InGaN/GaN epilayer top surface. The V-pits have six facets on $(1\bar{1}01)$ and a hexagonal shape on the top surface of the thin films. The depth and size of the V-pit defects depend on the InGaN layer thickness as shown in Fig. 1. Figure 1a shows a thick InGaN layer with high density of V-pits generated because of the annihilation of threading dislocations. Figure 1b shows a thicker layer with a higher density of V-pits and thus deeper thickness of V-pits. Figure 1c shows hexagonal shapes of V-pits on the top layers and on the c-plane (0001) as well as how these hexagonal defects can intersect with each other to initiate a continuous groove defect as indicated with black arrows.

The V-pit defects are generated because of complex relaxation mechanisms in the III-N layers. Due to the large strain mismatches between different

(Received June 27, 2020; accepted September 26, 2020; published online October 22, 2020)

layers, and with thicker III-N thin films, the strain energy increases in these III-N strained layers. At a certain thickness, the critical thickness, strained III-N thin films relax simultaneously with threading dislocations annihilation by forming V-pit defects.[3–10] Eldred et al.[10] used the semi-bulk approach to grow 20 periods of InGaN/GaN on Epi GaN on sapphire substrates. STEM results discussed the system relaxation mechanism that occurred through the propagation of threading dislocations on the Epi GaN layer and deflection of these dislocations in InGaN/GaN periods to finally form V-pit defects on the top surface of InGaN top layer; see Fig. 3 in Ref. 10. In this article, InGaN/GaN epilayers grown on both Si and sapphire substrates are assumed.

These defects affect the device performance, efficiency, and lifetime. Therefore, novel approaches to suppress threading dislocation growth in III-N systems are required. In the literature, several approaches have been pioneered and discussed;[11–16] specifically, the authors experimentally and numerically studied the effects of a novel approach, the embedded void approach (EVA), on decreasing the defect density in thin films in different III-N structures such as GaN-on-sapphire, GaN-on-Si and InGaN-on-Si.[11,12,14] EVA relies on introducing a huge number of elliptical micro-voids in the III-N layer close to the III-N/substrate interface. This huge number of micro-voids acts as a trapping zone close to the interface that decreases this flaw propagation. The experimental and numerical studies show a significant decrease in defect densities after using EVA.

The objective of this work is to facilitate the calculation of the optimum/critical layer thickness of thin films before forming the common V-pit defects on the surface of these structures. Thus, study of V-pit defect nucleation and growth by investigating the factors that affect the V-pit geometry and density during the growth of the InGaN/GaN epilayers on sapphire or Si substrates is critical. Notably, the model assumes an energy balance among the strain energy in the III-N layer, dislocation deterioration energy to form new V-pits, and the new V-pit facets energies that are generated as a result of the new facet formations. It also should be noted that, in this work, a single layer of III-N is assumed to be grown on a bulk substrate, whereas, in real structures, several periods of InGaN/GaN are grown on a bulk substrate. The thin-film layer is also assumed to have a cylindrical layer with a cone-shaped V-pit. Furthermore, the impact of using the embedded void approach in the current system with the developed model, to minimize the defect densities and therefore to minimize the generation of V-pit defects, is investigated.

METHODOLOGY

V-pit defects are generated because of the complex relaxation mechanism in III-N materials after exceeding the critical thickness, which can be calculated as Refs. 17,18:

$$h_c = \frac{b(1-\upsilon\cos^2\alpha)}{4\Pi\varepsilon(1+\upsilon)}\left[\ln\left(\frac{h_c}{b}\right)+1\right] \quad (1)$$

where b is the Burger vector, and υ is Poisson's ratio. From the first equation, a relation between the critical thickness and the misfit strains of the material is provided. After exceeding the critical thickness, the strain can be expressed as;

$$\varepsilon = \frac{b(1-\upsilon\cos^2\alpha)}{4\Pi h(1+\upsilon)}\left[\ln\left(\frac{h}{b}\right)+1\right] \quad (2)$$

Following Song,[19] a thermodynamic model is developed for the current systems by assuming bulk substrates. In this model, three different types of energies are assumed in a balanced system. The model is used to model the V-pit nucleation and growth. The energies are the strain energy in the III-N layer, dislocation deterioration energy to form the new V-pits, and V-pit facet energies that result because of facet formations.

As mentioned earlier, the V-pit is assumed to be a cone in a cylindrical domain with length h and radius R, while the V-pit has a radius a and height

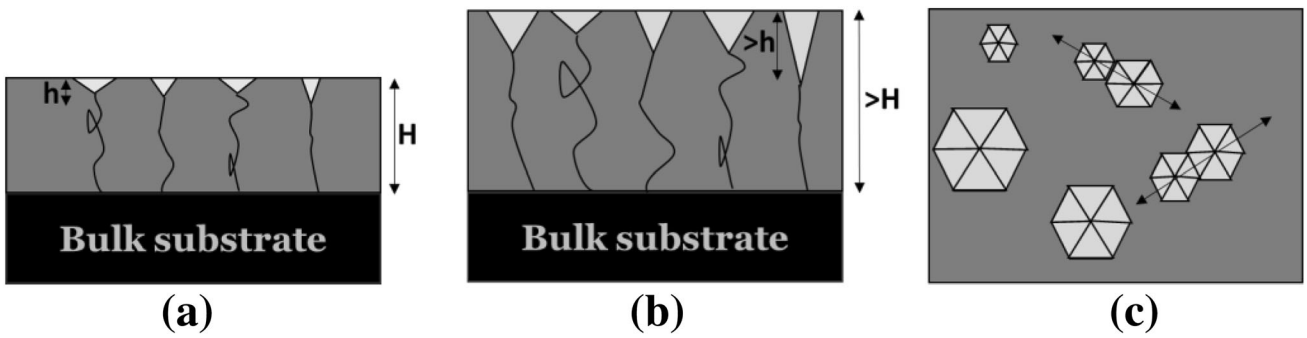

Fig. 1. (a) V-pit formation on the III-N layer top surface; (b) deeper and larger V-pit formation due to thicker III-N layers; (c) hexagonal top view faces on (0001); reprinted from Ref. 3.

h, as shown in Fig. 2. In this model, two balance systems have been assumed: (1) pre-nucleation of the V-pit; (2) post-nucleation of the V-pit. The result of these systems is the resulting energy because of the formation of the V-pit.

The total energy in the domain without V-pits can be calculated as:

$$E_{\text{pre}} = E_{\text{St}} + E_{\text{Dis}} \tag{3}$$

where E_{St} is the elastic strain energy and E_{Dis} is the dislocation energy[17,18]

$$E_S = -Ef^2 \Pi R^2 h \tag{4}$$

$$E_{\text{Dis}} = \frac{Gb^2(1-\upsilon\cos^2\alpha)}{2\Pi(1-\upsilon)}\left[\ln\left(\frac{R_D}{b}\right)+1\right]h \tag{5}$$

where E is Young's modulus, f is the misfit strain, and R_D is the cutoff radius of the threading dislocation.

The total energy in the domain with V-pits can be calculated as:

$$E_{\text{post}} = E_f + E_{\text{pit}} + E_{\text{sf}} \tag{6}$$

where E_f is the strain energy due to the facets forming, E_{pit} is the strain energy of the cone formation due to the material peel off, and E_{sf} is the surface energy due to the pit nucleation.

Hence, the required energy to nucleate V-pits is:

$$\Delta E = (E_f + E_{\text{pit}} + E_{\text{sf}}) - (E_{\text{St}} + E_{\text{Dis}}) \tag{7}$$

E_f can be calculated as the following:

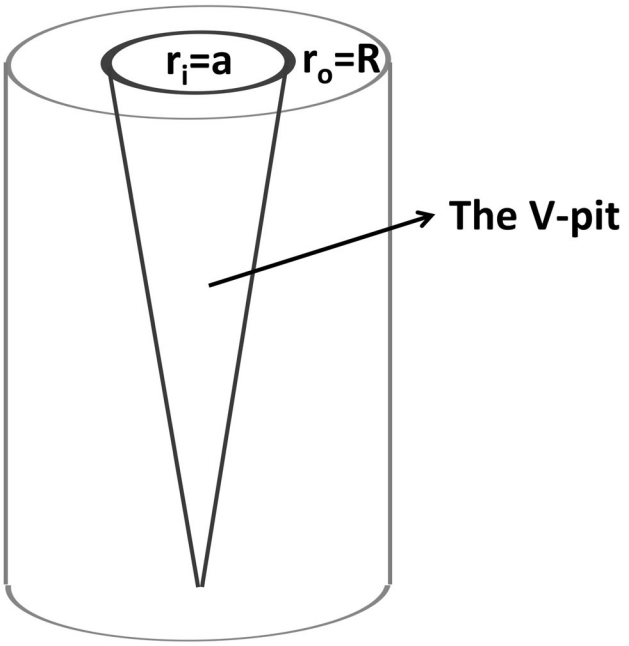

Fig. 2. Schematic figure reveals the V-pit (with a cone shape) with radius a and height h in a cylindrical domain with radius R; this figure is reprinted from Ref. 3.

$$E_\upsilon = \frac{1}{2}\sum_{i=1}^{3}\sum_{j=1}^{3}\sigma_{ij}\varepsilon_{ij} = \frac{1}{2}\sum_{k=1}^{6}\sum_{l=1}^{6}\sigma_k S_{kl}\sigma_l \tag{8}$$

In this work, bulk substrates are assumed. Normal, shear and peel stresses can be easily expressed from Suhir.[20] First, normal stresses can be expressed as:

$$\sigma_f(x) = Ef\left(1-e^{-k(1-x)}\right) \tag{9}$$

where $\kappa = \sqrt{\frac{1}{KEh}}$, $\kappa = \frac{2}{3}\left(\frac{1+\upsilon_s}{1-\upsilon_s}\right)\frac{h_S}{Y_S}$, and h_s is the substrate thickness (thick substrates), υ_s is the substrate Poisson's ratio, and E_s the substrate elastic modulus.

Then, shear stress $\tau(x)$ and peeling stress $p(x)$ can be expressed as:

$$\tau(x) = -Efhke^{-k(1-x)} \tag{10}$$

$$p(x) = -\frac{1}{2}Efh^2k^2e^{-k(1-x)} \tag{11}$$

Also E_{pit} and E_{sf} can be calculated as shown:

$$E_{\text{pit}} = Ef^2\left(\frac{1}{3}\Pi\frac{h^3}{d^2}\right) \tag{12}$$

$$E_{\text{sf}} = E\Pi\frac{h^2}{d^2}\sqrt{1+d} \tag{13}$$

From Eqs. 4, 5, 7, 12 and 13, the V-pit energy can be easily calculated.

RESULTS AND DISCUSSIONS

Results from the thermodynamics-based model are presented below for two different substrates, silicon and sapphire. In this article, $In_{0.65}Ga_{0.35}N$ is used on two different substrates to show the effects of lattice and thermal expansion coefficient mismatches on V-pit nucleation and growth. Thermal and mechanical parameters for InGaN, Si and sapphire are listed in Table I. Furthermore, results of the new approach, the embedded void approach (EVA), are presented to show how the EVA can decrease dislocation densities in thin films; consequently, the V-pit defect density will decrease.

The relation between the required energy to nucleate V-pits (the difference in the energies before and after the V-pit formation) and the III-N layer thickness assuming zero density of V-pits and high and low misfit strain values of 5×10^{-3} and 5×10^{-4}, respectively, is shown in Fig. 3. All the results are shown versus the thin-film layer thickness to be able to detect the critical thickness layer or the optimum thickness for the thin film before forming new V-pits. The energy has non-positive values because the second system, which contains V-pits, is greater than the first system, which

Table I. Thermal and mechanical parameters of InGaN, sapphire and Si[21,22]

Parameters	$In_{0.65}Ga_{0.35}N$	Sapphire	Si
Young's modulus, E(GPa)	186.5	400	168.9
Poisson's ratio, υ	0.353	0.33	0.262
α (K^{-1})	$\alpha_a = 3.646 \times 10^{-6}$ $\alpha_c = 3.44 \times 10^{-6}$	6.6×10^{-6}	2.6×10^{-6}

contains no V-pits. Based on the composition of InGaN used in this article, sapphire substrates have larger lattice and thermal expansion coefficient mismatches than silicon substrates. Therefore, for large strain mismatch values, and in the case of InGaN on sapphire substrates, the energy required to form the V-pits exponentially increased to reach around -5.5×10^{-8} J at 600 nm of the epilayer thickness, whereas, for the same strain mismatch value and in the case of InGaN on silicon substrates, the energy required to nucleate V-pits is relatively small (around -2×10^{-8} J) at the same epilayer thickness (600 nm). This shows how V-pits are directly related to lattice and thermal expansion coefficient mismatches between different layers, which responsible for generating threading dislocations. Furthermore, from Fig. 3, it should be noted that, in case of Si substrates, the thin film can be grown with thicker layers before having V-pit defects. For low strain mismatch values (5×10^{-4}) and in cases of both Si and sapphire substrates, the energy required to generate V-pits is relatively small, as expected. Therefore, the tendency of the materials to form V-pits is neglected.

The difference between energies before and after forming the V-pits versus the InGaN layer thickness is shown in Fig. 4. All the results are also shown versus the thin-film layer thickness to be able to detect the critical thickness layer or the optimum thickness for the thin film before forming new V-pits. In this case, a large strain mismatch value of 5×10^{-3} is used with different values of V-pit densities [1.0×10^6, 2.0×10^7, 3.0×10^7, 5.0×10^7 and 1.0×10^8 ($/cm^2$)]. Large strain mismatch in the system generates threading dislocations with high densities. As mentioned in the literature,[3,10] threading dislocations, generated at the interface between different layers, propagate to the top surface and are annihilated by forming common defects such as V-pits. Therefore, at low densities of V-pits ($1.0 \times 10^6/cm^2$), the energy required to form V-pits significantly increased, which refers to the high tendency to form such pits on the top surface of the thin film to relax the system. On the other hand, with high densities of V-pits ($1.0 \times 10^8/cm^2$), the energy required to form V-pits is relatively small and can be neglected, since the system has already formed larger V-pits with high density that have already relaxed the system. Therefore, there is no tendency to form new V-pits.

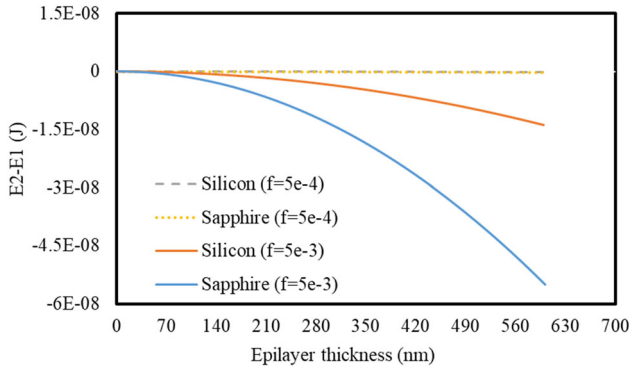

Fig. 3. The difference between energies before and after forming the V-pits versus the InGaN layer thickness assuming 5×10^{-3} and 5×10^{-4} misfit strains and no V-pits.

Figure 5 shows the difference between energies before and after forming the V-pits versus the InGaN layer thickness. In these results, no V-pits or different values of strain mismatch ($1.0 \times 10^{-7}, 1.0 \times 10^{-6}, 1.0 \times 10^{-5}, 1.0 \times 10^{-4}$ and 1.0×10^{-3}) are assumed. With very low values of strain mismatch ($1.0 \times 10^{-7}, 1.0 \times 10^{-6}$ and 1.0×10^{-5}), the energy required to form V-pits is low and can be neglected. However, with high values of strain mismatch that generate high threading dislocation densities, the energy values required to form V-pits are huge, since there are no V-pits in the system. Overall, the results show that, at the beginning of the growth of InGaN/GaN on either Si or sapphire where there are no V-pits in the system as well as with high strain mismatch between different layers (depending on the different layers), the tendency of the system to relax is high, where the only way to relax it by forming V-pits.

Therefore, to limit the generation of V-pits by decreasing defect densities in thin films, novel approaches such as EVA can be used. In previous work, the authors experimentally and numerically studied the effects of EVA on different systems such as GaN-on-sapphire, GaN-on-Si and InGaN-on-Si,[11,12,14,23] where EVA showed significant contributions to decreasing threading dislocation densities on the top layer of thin films. For example, modeling EVA on the system of InGaN-on-Si is shown in Fig. 6. EVA is simulated in a repeat unit cell (RUC) structure with periodic boundary conditions (PBCs). EVA is modeled using a commercial

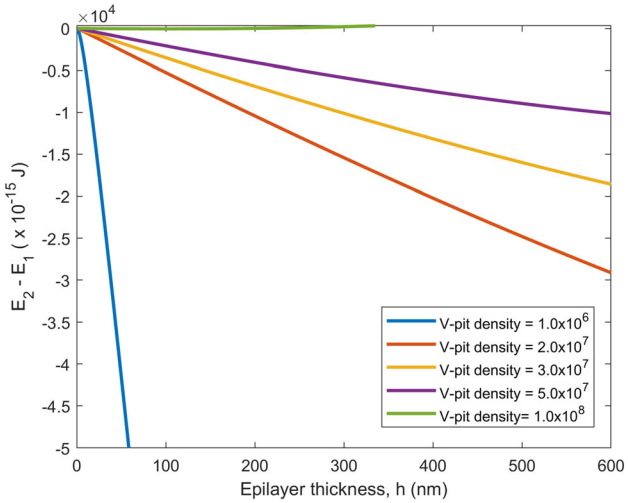

Fig. 4. The difference between energies before and after forming the V-pits versus the InGaN layer thickness assuming the same misfit strain (5×10^{-3}) and different V-pit densities (1.0×10^6, 2.0×10^7, 3.0×10^7, 5.0×10^7 and $1.0 \times 10^8/cm^2$).

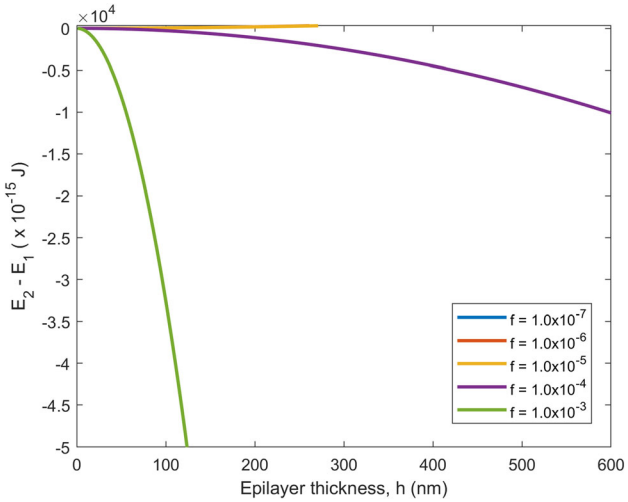

Fig. 5. The difference between energies before and after forming the V-pits versus the InGaN layer thickness assuming no initial V-pit density and different misfit strains $(1.0 \times 10^{-7}, 1.0 \times 10^{-6}, 1.0 \times 10^{-5}, 1.0 \times 10^{-4}, 1.0 \times 10^{-3})$.

finite element solver considering the crystal orientations and slip systems of each material as well as under the realistic experimental growth conditions of the system. For more details, see Khafagy et al.[11,12] Fig. 6a and b shows von-Mises stress and total shear strain contours, where the embedded void affects the cell structure by decreasing the stresses on the boundary of the cell structure (along the void height). A significant decrease in stresses between the embedded void reduces dislocation velocity in these zones, which suppresses threading dislocations produced on the interface. Moreover, due to the high values of stress close to the embedded void boundaries, such voids act as a sink to the threading dislocations moving up from the interface. Figure 6c shows stress values measured at the right edge of the cell structure, where the stress curve of the results without the embedded void shows the stress concentration at the interface as a result of large thermal expansion coefficient mismatches between the two layers. The stress curve of the results with the embedded void shows the significant drop of stresses at the void regions, which proves that decreasing dislocation velocity in this region is expected. Therefore, using this approach can significantly affect the nucleation and growth of V-pit defects. Future work will be conducted to explicitly consider the crystal structure orientations of each layer and threading dislocation densities as well as integrate the EVA with the thermodynamics-based model on different III-N structures.

CONCLUSION

Large mismatch of both lattice and thermal expansion coefficients of III N epi-layers and their substrates forms defects with high densities. These defects, such as threading dislocations, propagate under the growth conditions of the system and are annihilated, after exceeding the thin-film critical thickness, to relax the system by forming common defects, V-pit defects, on the top surface of the top layer. These defects affect the reliability, lifetime and performance of devices. Several approaches, such as the embedded voids approach, have been introduced to the literature to minimize these threading dislocations. In this work, we present the common V-pit defect nucleation and growth by considering the factors that impact the V-pit size and density during the growth of the InGaN/GaN epilayers on either sapphire or Si substrates. Furthermore, the impact of the embedded void approach on minimizing the defect densities and therefore the surface roughness is discussed. This can significantly facilitate the costly experiments in the calculation of the optimum/maximum thin-film layer thickness before forming new V-pits on the top of the structures.

Results show that V-pit nucleation and growth are affected by misfit strain between both different layers and the thin-film layer thickness. With large misfit strain and zero initial value of the V-pit density, the system with thicker thin-film layers requires relaxing by forming high density V-pits. However, with higher densities of V-pits and higher misfit strain values, the system is already relaxed with the assumed initial values of the V-pits; therefore, there is no tendency to generate more V-pits. Results of different substrates show an excellent comparison that proves how the thermal expansion coefficient and lattice mismatches directly affect the V-pit formation and growth. In the current system, Si substrates are the better choice for $In_{0.65}Ga_{0.35}N$ than sapphire substrates.

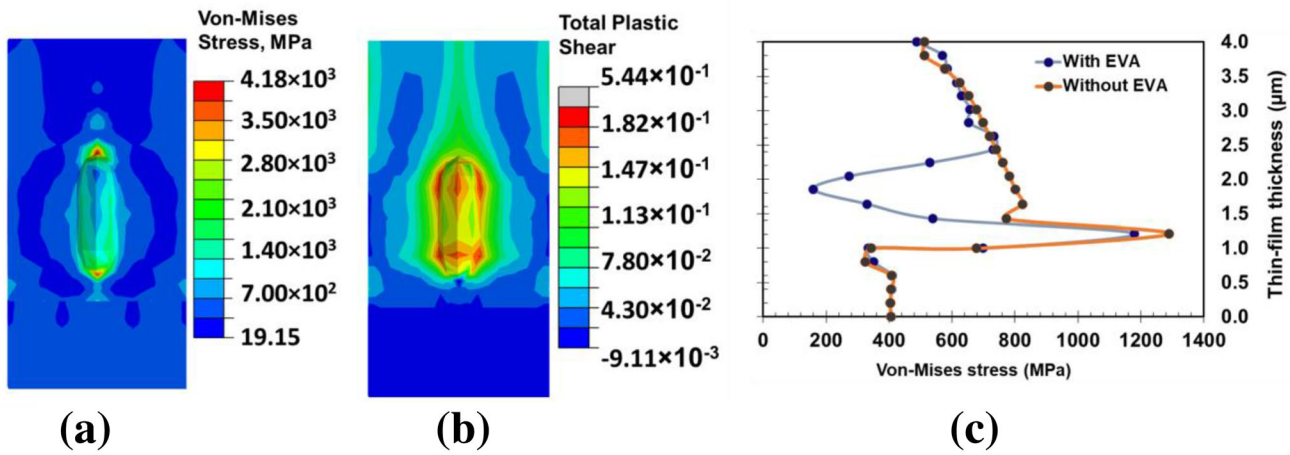

Fig. 6. Effects of EVA on decreasing threading dislocation densities; (a) von-Mises stress contour; (b) total plastic shear strain contour; (c) von-Mises stresses along the thickness curve in both cases, with and without embedded voids (data from Ref. 11).

ACKNOWLEDGEMENTS

The support from the Young Investigators Research Grant (No. YIRG05) at the British University in Egypt and the Research Grant from the Academy of Scientific Research & Technology (ASRT) are greatly appreciated.

CONFLICT OF INTEREST

The authors declare that they have no conflict of interest.

REFERENCES

1. J. Cheng, X. Yang, L. Sang, L. Guo, J. Zhang, J. Wang, C. He, L. Zhang, M. Wang, F. Xu, N. Tang, Z. Qin, X. Wang, and B. Shen, *Sci. Rep.* 6, 23020 (2016).
2. S.A. Kukushkin, A.V. Osipov, V.N. Bessolov, B.K. Medvedev, V.K. Nevolin, and K.A. Tcarik, *Rev. Adv. Mater. Sci.* 17, 1 (2008).
3. K.H. Khafagy, T.M. Hatem, and S.M. Bedair, in *TMS 2020 149th Annual Meeting & Exhibition Supplemental Proceedings* (Springer US, 2020), pp. 2057–2064.
4. J.E. Northrup, L.T. Romano, and J. Neugebauer, *Appl. Phys. Lett.* 74, 2319 (1999).
5. J.E. Northrup and J. Neugebauer, *Phys. Rev. B Condens. Matter Mater. Phys.* 60, 8473 (1999).
6. A.V. Lobanova, A.L. Kolesnikova, A.E. Romanov, S.Y. Karpov, M.E. Rudinsky, and E.V. Yakovlev, *Appl. Phys. Lett.* 103, 152106 (2013).
7. W. Qi, J. Zhang, C. Mo, X. Wang, X. Wu, Z. Quan, G. Wang, S. Pan, F. Fang, J. Liu, and F. Jiang, *J. Appl. Phys.* 122, 084504 (2017).
8. X.H. Wu, C.R. Elsass, A. Abare, M. MacK, S. Keller, P.M. Petroff, S.P. Denbaars, J.S. Speck, and S.J. Rosner, *Appl. Phys. Lett.* 72, 692 (1998).
9. J. Kim, Y.-H. Cho, D.-S. Ko, X.-S. Li, J.-Y. Won, E. Lee, S.-H. Park, J.-Y. Kim, and S. Kim, *Opt. Express* 22, A857 (2014).
10. T.B. Eldred, M. Abdelhamid, J.G. Reynolds, N.A. El-Masry, J.M. Lebeau, and S.M. Bedair, *Appl. Phys. Lett.* 116, 102104 (2020).
11. K.H. Khafagy, T.M. Hatem, and S.M. Bedair, *Appl. Phys. Lett.* 112, 042109 (2018).
12. K.H. Khafagy, T.M. Hatem, and S.M. Bedair, *MRS Adv.* 4, 755 (2019).
13. K.H. Khafagy, T.M. Hatem, and S.M. Bedair, in *TMS 2020 147th Annual Meeting & Exhibition Supplemental Proceedings* (Springer US, 2018), pp. 453–461.
14. S.I. Salah, T.M. Hatem, E.E. Khalil, and S.M. Bedair, *Mater. Sci. Eng., B* 242, 104 (2019).
15. Y.A. Bioud, A. Boucherif, M. Myronov, A. Soltani, G. Patriarche, N. Braidy, M. Jellite, D. Drouin, and R. Arès, *Nat. Commun.* 10, 1 (2019).
16. Y.A. Biouda, A. Boucherifa, M. Myronovb, G. Patriarchec, D. Drouina, and R. Arèsa, *Trans. ECS* 93, 81 (2019).
17. F.C. Frank, *Lond. Edinb. Dublin Philos. Mag. J. Sci.* 42, 809 (1951).
18. J. Matthews, *Epitaxial Growth Part A* (Amsterdam: Elsevier, 2012).
19. T.L. Song, *J. Appl. Phys.* 98, 084906 (2005).
20. E. Suhir, *J. Appl. Mech.* 64, 15 (2017).
21. H. Morkoç, *Handbook of Nitride Semiconductors and Devices, Materials Properties, Physics and Growth*, 1st ed. (New York: Wiley, 2009).
22. M.K. Horton, S. Rhode, S.L. Sahonta, M.J. Kappers, S.J. Haigh, T.J. Pennycook, C.J. Humphreys, R.O. Dusane, and M.A. Moram, *Nano Lett.* 15, 923 (2015).
23. P. Frajtag, N.A. El-Masry, N. Nepal, and S.M. Bedair, *Appl. Phys. Lett.* 98, 023115 (2011).